inorganics

MDPI

Article

Manganese(I)-Based CORMs with 5-Substituted 3-(2-Pyridyl)Pyrazole Ligands

Ralf Mede, Steve Gläser, Benedikt Suchland, Björn Schowtka, Miles Mandel, Helmar Görls, Sven Krieck, Alexander Schiller and Matthias Westerhausen *

Institute of Inorganic and Analytical Chemistry, Friedrich Schiller University Jena, Humboldtstrasse 8, 07743 Jena, Germany; ralf.mede@uni-jena.de (R.M.); glaeser.steve@gmail.com (S.G.); benedikt.suchland@uni-jena.de (Be.S.); schowtka@t-online.de (Bj.S.); miles.mandel@uni-jena.de (M.M.); helmar.goerls@uni-jena.de (H.G.); Sven.Krieck@uni-jena.de (S.K.); alexander.schiller@uni-jena.de (A.S.)
* Correspondence: m.we@uni-jena.de; Tel.: +49-3641-948-110

Academic Editor: Lígia M. Saraiva
Received: 19 December 2016; Accepted: 19 January 2017; Published: 25 January 2017

Abstract: The reaction of $[(OC)_5MnBr]$ with substituted 3-(2-pyridyl)pyrazoles) 2-$PyPz^RH$ (**1a-l**) in methanol or diethyl ether yields the yellow to orange manganese(I) complexes $[(OC)_3Mn(Br)(2\text{-}PyPz^RH)]$ (**2a-l**), the substituents R being phenyl (**a**), 1-naphthyl (**b**), 2-anthracenyl (**c**), 1-pyrenyl (**d**), 4-bromophenyl (**e**), 3-bromophenyl (**f**), duryl (**g**), 2-pyridyl (**h**), 2-furanyl (**i**), 2-thienyl (**j**), ferrocenyl (**k**), and 1-adamantyl (**l**). The carbonyl ligands are arranged facially, leading to three chemically different CO ligands due to different *trans*-positioned *Lewis* donors. The diversity of the substituent R demonstrates that this photoCORM backbone can easily be varied with a negligible influence on the central $(OC)_3MnBr$ fragment, because the structural parameters and the spectroscopic data of this unit are very similar for all these derivatives. Even the ferrocenyl complex **2k** shows a redox potential for the ferrocenyl subunit which is identical to the value of the free 5-ferrocenyl-3-(2-pyridyl)pyrazole (**1k**). The ease of variation of the starting 5-substituted 3-(2-pyridyl)pyrazoles) offers a modular system to attach diverse substituents at the periphery of the photoCORM complex.

Keywords: CORMs; photoCORMs; manganese carbonyls; pyridylpyrazoles; manganese pyrazolates

1. Introduction

Carbon monoxide releasing molecules (CORMs) are compounds that liberate the signaling molecule CO for medicinal and biological administration. Metal carbonyls are usually considered for this purpose because numerous carbonyl ligands can be transported to a predetermined disease site and liberated via diverse triggers. Thus, CORMs are distinguished by the liberation initiators such as enzymes (ET-CORMs), illumination (photoCORMs), pH change, or substitution reactions (for recent reviews see [1–17]). Especially photoCORMs represent a prominent group because a clean delivery of CO seems to be possible without the necessity to add another chemical trigger [8,13–15]. Due to the fact that exaggerated light-sensitivity hampers handling and administration of carbon monoxide whereas short wave wavelengths are harmful for cells, a balance has to be considered. Limitation of toxic side effects of CORMs can be expected if essential metals such as late 3d metals are used. The prevalent essential 3d metal is iron [18–21], however, the redox chemistry of iron is quite challenging, known as *Fenton* chemistry [21]. The most convenient element is manganese and no toxicity is related to this transition metal in concentrations, relevant for medicinal administration of carbon monoxide [22]. Thus, many manganese-based CORMs have been studied and a very low toxicity has been observed. In addition, diverse ligands can be used to guarantee solubility in aqueous media and influence CO release triggers. The carbonyl ligands must be in a facial arrangement in order

to ensure stability in aqueous solutions. If four CO ligands are bound at octahedrally coordinated Mn centers, one of the *trans*-positioned carbonyl ligands is easily substituted by *Lewis* bases such as ethers or dimethylsulfoxide (DMSO) [23].

Solubility of CORMs in aqueous media often is advantageous for administration of CO. However, immobilized CORMs increasingly gain attention and diverse concepts exist to administer carbon monoxide from such insoluble CORMs [24,25]. As a representative example, insoluble CORMs can be embedded in matrices [3] such as non-wovens [26,27] and CO is released upon illumination whereas the degradation products remain in the polymer matrices and, hence, the hazard potential of metal-containing degradation products plays an insignificant role. For soluble CORMs, low toxicity is required for the CORMs as well as for their degradation end-products after CO release. In all these manganese(I)-based CORMs, the metal centers show a low spin state in an octahedral environment with a d^6 configuration. During CO liberation, most commonly an oxidation to manganese(II) has been observed. In buffered aqueous solutions, manganese(II) hydrogenphosphate $MnHPO_4$ of low toxicity has been identified after CO release from dinuclear $[\{(OC)_3Mn\}_2(\mu\text{-}SC_2H_4NH_3)_3]Br_2$ (CORM-EDE1 [28]).

In the past many ligand systems have been tested to tune diverse properties of manganese(I)-based CORMs such as e.g., solubility in water, nature of trigger, color, non-toxicity, stability under aerobic conditions, and CO release kinetics. Schatzschneider and coworkers [29,30] already demonstrated at complexes with a cationic $[(OC)_3Mn(Pz_3C\text{-}R)]$ unit (Pz = pyrazolyl) that alterations at the periphery and immobilization at SiO_2 surfaces or peptides have negligible influence on the photochemical CO release properties. In this study, we present a flexible modular system that allows to attach diverse functional groups at the periphery of 3-(2-pyridyl)pyrazole ligands which are known to act as strong bidentate *Lewis* bases [31] whereas the central manganese carbonyl unit remains nearly unaffected. Based on our extensive experience with 5-substituted 3-(2-pyridyl)pyrazoles (2-$PyPz^RH$, **1**; see Scheme 1 [32,33]), we screened manganese(I)-based photoCORMs with these bidentate ligands at a 14-electron $(OC)_3MnBr$ moiety to demonstrate the variability of this substance class.

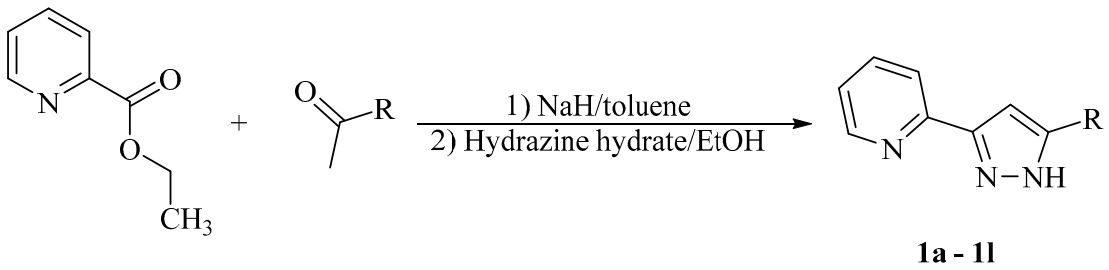

Scheme 1. Synthesis of 5-substituted 3-(2-pyridyl)pyrazoles) 2-$PyPz^RH$ from 2-pyridylcarboxylic esters and ketones allowing a wide variety of substituents R at the 5-position of the pyrazole ring.

2. Results

*2.1. Synthesis of [(OC)$_3$Mn(Br)(2-PyPz^{R}H)] (**2**)*

Easily available $[(OC)_5MnBr]$ readily reacts with the substituted 3-(2-pyridyl)pyrazoles **1** in methanol or diethyl ether yielding the corresponding yellow to orange manganese(I) complexes **2** as shown in Scheme 2. In all these complexes, the carbonyl ligands are arranged facially, leading to three chemically different CO ligands due to different *trans*-positioned *Lewis* donors. In Table 1, the 5-positioned group R is defined and selected spectroscopic parameters are summarized.

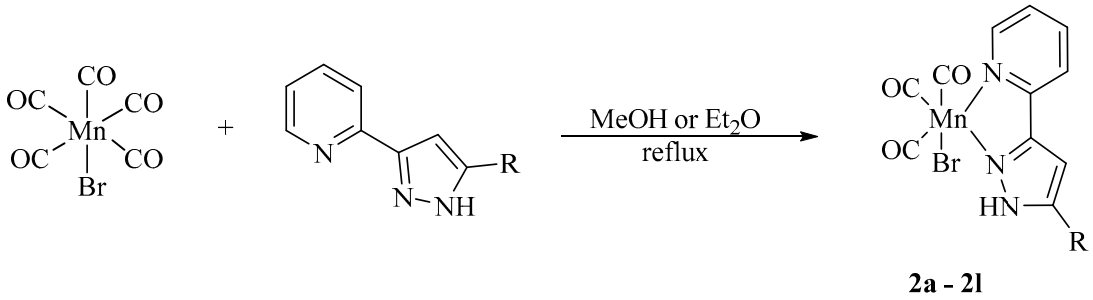

2a - 2l

Scheme 2. Synthesis of the [$(OC)_3$Mn(Br)(2-PyPz^{R}H)] (**2**) from substituted 3-(2-pyridyl)pyrazoles and [$(OC)_5$MnBr].

Table 1. Selected spectroscopic data of the carbonyl ligands of [$(OC)_3$Mn(Br)(2-PyPz^{R}H)] (**2**). The group R is bound in 5-position of the bidentate 3-(2-pyridyl)pyrazole ligand.

Complex	R [1]	$\delta(^{13}C_{CO}\{^1H\})$/ppm	ν(CO)/cm^{-1}
2a	Ph	223.5, 223.9	2021, 1895
2b	1-Naph	223.8, 223.3, 221.5	2026, 1948, 1912
2c	2-Anth	n.o.[2]	2023, 1931, 1904
2d	1-Pyr	n.o. [2]	2027, 1930, 1898, 1864
2e	C_6H_4-4-Br	228.5, 226.3	2020, 1940, 1906, 1886
2f	C_6H_4-3-Br	223.2, 221.5	2024, 1914, 1862, 1838
2g	C_6H-2,3,5,6-Me_4 (Dur)	222.9, 220.6	2022, 1940, 1902
2h	2-Py	222.3, 221.2, 220.9	2024, 1932, 1892
2i	2-Fu	n.o. [2]	2024, 1933, 1895
2j	2-Thi	n.o. [2]	2020, 1910
2k	Fc	224.1, 223.5, 221.9	2023, 1931, 1911, 1866
2l	1-Ad	n.o. [2]	2030, 1943, 1913, 1893

[1] Abbreviations: Phenyl Ph, Naph naphthyl, anthracenyl Ant, pyrenyl Pyr, duryl Dur, pyridyl Py, furanyl Fu, thienyl Thi, ferrocenyl Fc, adamantyl Ad; [2] Not observed.

The influence of the substituent R on the spectroscopic parameters of the carbonyl ligands is very small. The chemical shifts $\delta(^{13}C_{CO}\{^1H\})$ lie in the very narrow range between 220 and 229 ppm, even though that two CO ligands are *trans*-positioned to strong sp^2-hybridized nitrogen donors whereas the third carbonyl is *trans*-arranged to a rather weakly donating bromide. Commonly, the resonances of the carbonyl ligands are broadened or in some cases even unobservable. The IR stretching vibrations ν(CO) of the carbonyls show characteristic bands around 2025, 1935 and 1900 cm^{-1}, however, the number of observed bands varies due to overlap. These findings support that the substituent R at the pyrazole ring has a negligible influence on the properties of the manganese(I) carbonyl fragment allowing large variations in order to incorporate functional groups for diverse applications. Even complexes with a second strong *Lewis* base such as another 2-pyridyl group (complex **2h**) or the bulky redox-active ferrocenyl substituent (complex **2k**) exhibit very similar spectroscopic data.

The crystal structures also verify that the central $(OC)_3$MnBr remained nearly unaffected by the substitution pattern of the pyrazole ring. Selected structural parameters of the manganese(I) carbonyls are listed in Table 2. Representative molecular structures are depicted in Figures 1 and 2 for the complexes **2f** and **2k**, respectively. The molecular representations and numbering schemes of the other manganese(I)-based photoCORMs are depicted in the Supporting Information. The N-bond hydrogen atom at the pyrazole ring is able to form hydrogen bridges to methanol or THF which are maintained also in the solid state. Two representative examples are the derivatives **2f** and **2k** that are depicted in Figures 1 and 2, other methanol adducts can be found in the Supporting Information.

Table 2. Selected bond lengths (pm) of the complexes $[(OC)_3Mn(Br)(2\text{-}PyPz^RH)]$ (**2**). The group R is bound in 5-position of the bidentate 3-(2-pyridyl)pyrazole ligand (definition of R see Table 1).

Complex	Mn1–Br1	Mn1–$C_{trans\,Py}$	Mn1–$C_{trans\,Pz}$	Mn1–$C_{trans\,Br}$	Mn1–N_{Py}	Mn1–N_{Pz}
2a	252.43(5)	182.2(3)	181.5(3)	186.5(3)	208.2(2)	202.9(2)
2b	254.00(11)	180.9(6)	181.3(6)	180.9(6)	207.9(5)	202.4(5)
2e	254.20(5)	181.3(3)	180.7(3)	180.3(3)	208.2(2)	203.1(2)
2f	253.86(4)	182.0(3)	179.9(3)	179.7(3)	206.9(2)	201.9(2)
2g	254.97(4)	181.0(2)	181.4(2)	180.6(2)	207.60(16)	203.58(16)
2h	253.78(4)	182.4(2)	180.4(2)	180.6(2)	208.32(17)	202.83(17)
2i	255.38(4)	181.5(2)	181.0(2)	180.4(2)	207.72(19)	203.36(19)
2j	255.66(4)	181.8(3)	181.0(3)	181.2(3)	207.8(2)	202.20(18)
2k	254.78(9)	181.4(5)	180.5(5)	181.5(5)	206.8(4)	201.7(4)

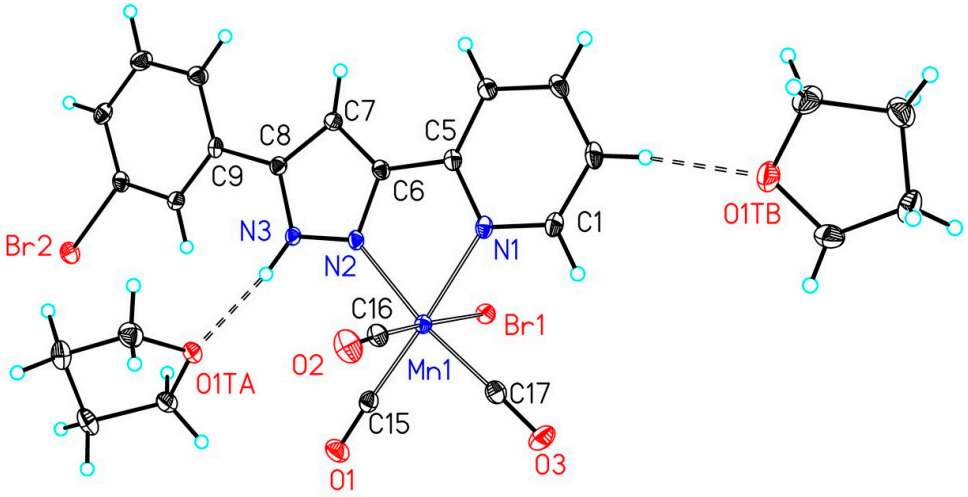

Figure 1. Molecular structure and numbering scheme of **2f**·2THF. The ellipsoids represent a probability of 30%, H atoms are drawn with arbitrary radii. Selected bond lengths are listed in Table 2.

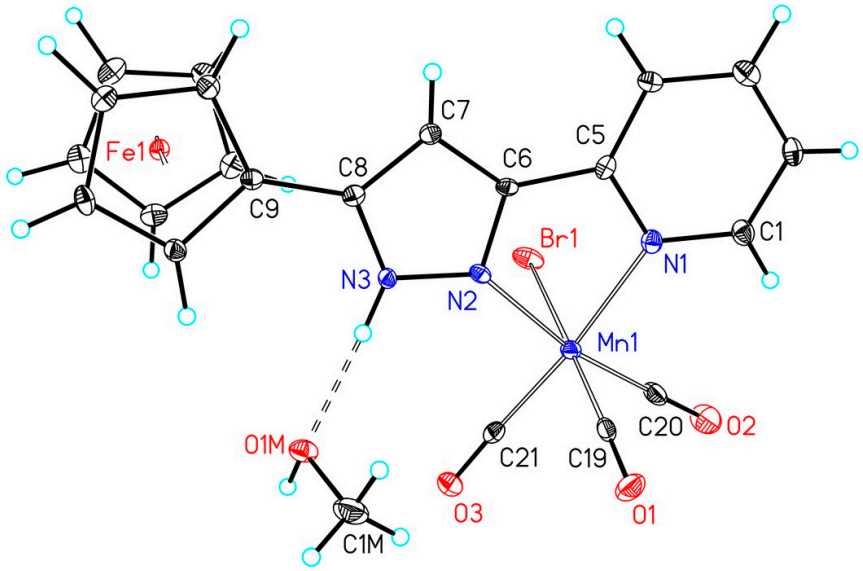

Figure 2. Molecular structure and numbering scheme of **2k**·MeOH. The ellipsoids represent a probability of 30%, H atoms are shown with arbitrary radii. Selected bond lengths are listed in Table 2.

The Mn1–Br1 bond lengths vary in a very narrow region between 252.43(5) (**2a**) and 255.66(4) pm (**2j**). The Mn1–N_{Py} distances to the pyridyl bases are significantly larger than the Mn1–N_{Pz} values to the pyrazole donors. Due to the *trans* influence the shorter Mn1–N_{Pz} bond leads in most cases to elongated Mn1–$C_{trans\,Pz}$ bonds to the *trans* arranged carbonyls, however, this effect lies within the uncertainty of the distances. Slightly shorter Mn1–$C_{trans\,Br}$ bond lengths are also found for the carbonyls in *trans* position to the bromine atom. A shorter Mn1–C bond is indicative for a stronger back donation from the metal to the π*(CO) orbital of the carbonyl ligand weakening the corresponding CO bond. For the phenyl-substituted derivative **2a** a larger Mn1–$C_{trans\,Br}$ of 186.5(3) pm is found whereas all other complexes show significantly shorter Mn1–C bonds around 181 pm in a very narrow range. In agreement with the IR vibrations of the carbonyls, which are very similar for all complexes, this finding is an artefact due to a slight disorder of Br1 and the *trans* arranged carbonyl ligand; however, it was impossible to resolve this two-site disordering. As a consequence of this disordering, the ellipsoid of C16 is oriented along the Mn1–C16–O2 unit (see Supporting Information).

2.2. Degradation of [(OC)$_3$Mn(Br)(2-PyPz^{R}H)] (R = Ph, Naph) in Methanol

The degradation of the photoCORMs **2a** and **2b** were studied to shed light on the final decomposition end-products after release of all carbonyl ligands (see next Chap. 2.3). As observed in earlier studies [28,34–36], the CO liberation is accompanied by oxidation processes and the formation of paramagnetic manganese(II) complexes. The formation of open shell systems impeded an NMR spectroscopic monitoring of the degradation reaction. Therefore, we limited the characterization of the end products on mass spectrometry, X-ray crystal determination, and IR studies. The latter verified that all carbon monoxide molecules were released. The degradation was investigated in methanol and we were able to obtain single crystals for X-ray diffraction experiments. As representative examples we studied the degradation of the two complexes [(OC)$_3$Mn(Br)(2-PyPz^{R}H)] [R = Ph (**2a**), Naph (**2b**)] in methanol at daylight, yielding tetranuclear manganese(II) (R = Ph, **3a**) and mixed manganese(II)/manganese(III) (R = Naph, **3b**) compounds according to Schemes 3 and 4, respectively.

The molecular structure and numbering scheme of [$Mn_4(Br)_2(OMe)_2$(2-PyPz^{Ph})$_4$] (**3a**) is shown in Figure 3. Symmetry-related atoms are marked with the letter A. All manganese atoms in this centrosymmetric complex show an oxidation state of +II. The methoxide anions occupy μ_3-bridging positions between three Mn centers. The Mn2 atom is in a distorted tetrahedral environment, whereas Mn1 shows a distorted octahedral coordination sphere. The pyrazolate anions bind to two manganese(II) ions.

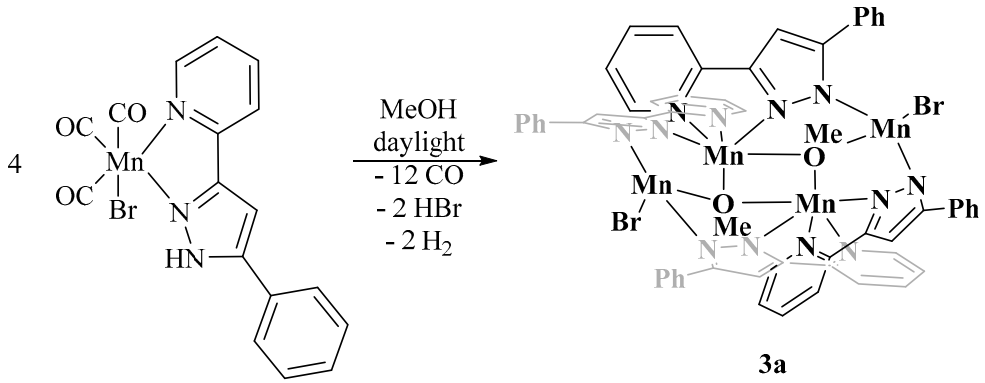

Scheme 3. Degradation of [(OC)$_3$Mn(Br)(2-PyPz^{Ph}H)] (**2a**) at daylight and room temperature in methanol yielding [$Mn_4(Br)_2(OMe)_2$(2-PyPz^{Ph})$_4$] (**3a**).

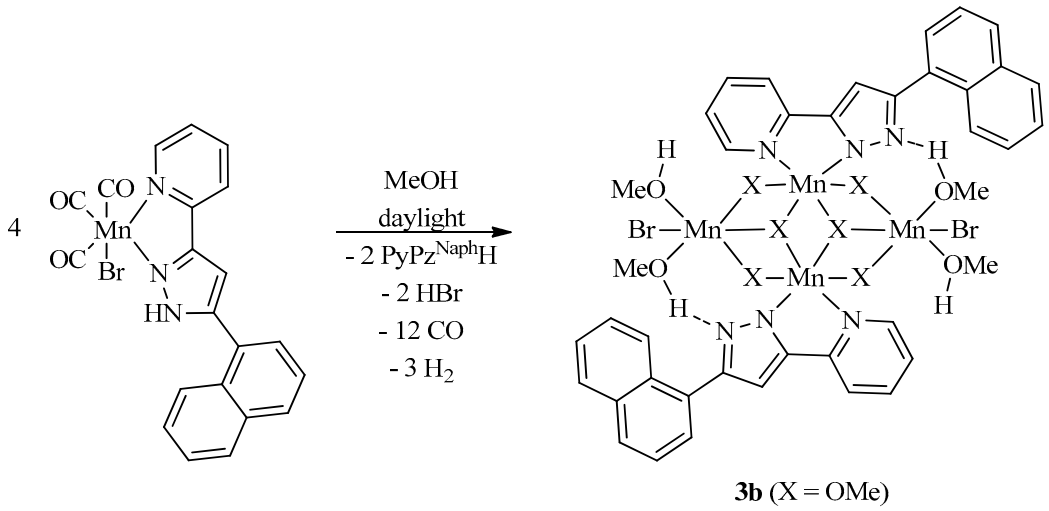

Scheme 4. Degradation of $[(OC)_3Mn(Br)(2\text{-}PyPz^{Naph}H)]$ (**2b**) at daylight and room temperature in methanol yielding $[(MeOH)_4Mn_4(Br)_2(OMe)_6(2\text{-}PyPz^{Naph})_2]$ (**3b**).

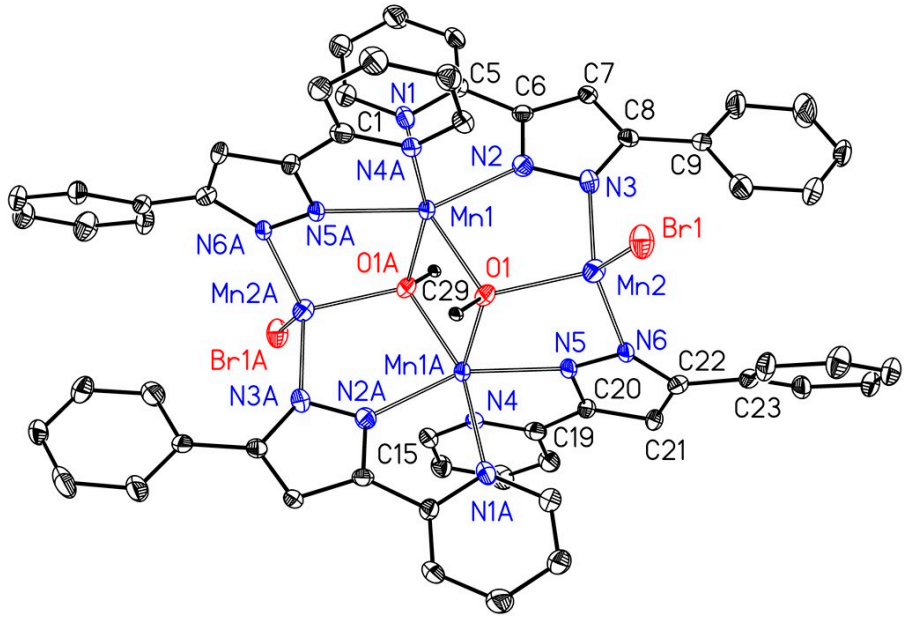

Figure 3. Molecular structure and numbering scheme of $[Mn_4(Br)_2(\mu_3\text{-}OMe)_2(2\text{-}PyPz^{Ph})_4]$ (**3a**). The ellipsoids represent a probability of 30%, H atoms are neglected for clarity reasons.

The molecular structure and numbering scheme of the mixed-valent centrosymmetric complex $[(MeOH)_4Mn_4(Br)_2(OMe)_6(2\text{-}PyPz^{Naph})_2]$ (**3b**) is depicted in Figure 4; again symmetry related atoms are marked with the letter A. Two methoxide ligands occupy μ_3- and four methoxide ions μ_2-bridging positions. All manganese atoms are embedded in distorted octahedral environments.

As observed earlier, degradation of manganese(I)-based photoCORMs upon illumination is accompanied by redox processes [28,34–36], yielding carbonyl-free manganese(II) and manganese(III) complexes or even manganese oxide species. Due to degradation in methanol in an inert atmosphere, methoxides and pyrazolates are observed. In $[Mn_4(Br)_2(\mu_3\text{-}OMe)_2(2\text{-}PyPz^{Ph})_4]$ (**3a**) all manganese atoms have an oxidation state of +II, however, Mn1 is in a distorted octahedral and Mn2 in a distorted tetrahedral environment. An average Mn–O bond length of 219.4 pm is observed with a slightly smaller value for Mn2–N3 of 213.4(4) pm. The higher oxidation state of +II leads to a slight shortening

of the Mn2–Br1 bond (246.9(1) pm) compared to derivatives **2** (average Mn^{I}–Br 254.3 pm) due to an enhanced electrostatic attraction and a smaller coordination number.

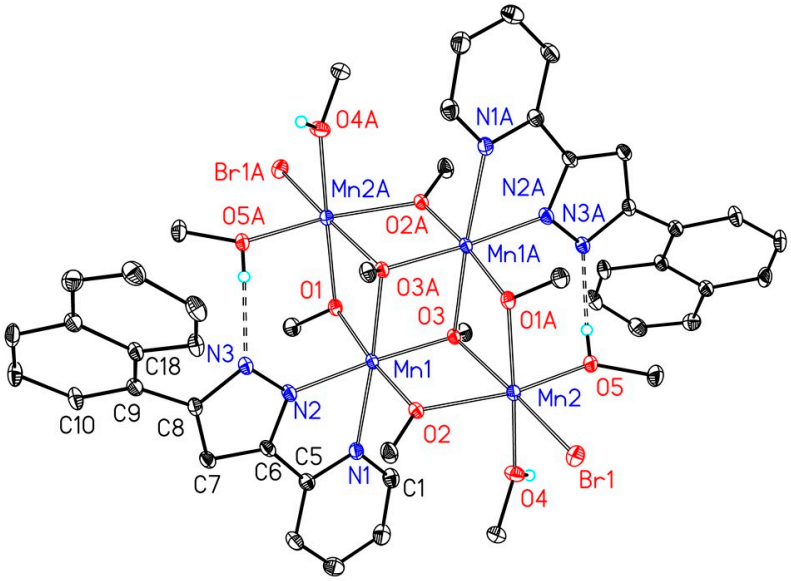

Figure 4. Molecular structure and numbering scheme of $[(MeOH)_4Mn_4(Br)_2(OMe)_6(2\text{-}PyPz^{Naph})_2]$ (**3b**). The ellipsoids represent a probability of 30%, H atoms are omitted for the sake of clarity with the exception of those of the ligated methanol molecules.

The degradation product $[(MeOH)_4Mn_4(Br)_2(\mu_3\text{-}OMe)_2(\mu\text{-}OMe)_4(2\text{-}PyPz^{Naph})_2]$ (**3b**) is a mixed valent complex with Mn^{II} and Mn^{III} atoms in distorted octahedral environments. The μ-bridging methoxide anions bridge Mn^{II} and Mn^{III} atoms, leading to significantly different distances of 189.2(3) pm for Mn1–O1 and 217.2(3) pm for Mn2A–O1. A similar situation is observed for O2 (Mn1–O2 190.0(3), Mn2–O2 213.5(3) pm). These bonding parameters clearly allow to assign Mn1 to the oxidation state of +III and Mn2 to +II. In agreement with this interpretation, the soft bromide ion binds to the softer Mn2 atom with a Mn2–Br1 distance of 262.16(7) pm; this value is larger than the Mn–Br distance of complex **3a** due to the enhanced coordination number. In addition to the anionic ligands also four ligated methanol molecules saturate the coordination spheres of the Mn^{II} atoms Mn2 and Mn2A, two of them form hydrogen bridges to the pyrazolate ions.

*2.3. CO Release from $[(OC)_3Mn(Br)(2\text{-}PyPz^{Ph})]$ (**2**)*

It has been shown earlier that manganese(I) complexes containing the 14-electron $(OC)_3MnBr$ moiety represent valuable photoCORMs. In order to also demonstrate the suitability of these complexes, as a representative example the CO release of **2a** was investigated at the solid phase. The amount of liberated CO was detected and quantified with a portable CO sensor (Dräger Pac7000, Drägerwerk AG &Co. KGaA, Lübeck, Germany) during illumination with LED lamps in a closed desiccator, as described elsewhere [26]. The measurements were performed with two different wavelengths (365 and 480 nm) and liberated CO was quantified as number of released CO molecules per CORM. Illumination of **2a** at 365 nm for 30 min led to liberation of 0.086 CO molecules per manganese(I) carbonyl complex, referring to t_{30min} = 0.086 CO/photoCORM (see Figure 5). When the experiments were accomplished at 480 nm, 0.089 CO molecules per CORM were released, giving a value of t_{30min} = 0.089 CO/photoCORM. The small number of released carbon monoxide molecules is caused by the fact that only carbonyl complexes at the surface are degraded by this procedure. After stirring of the remaining solid, further CO can be released. In methanol solution the CO release is much faster and quantitative (see Figure S4 in the Supporting Information).

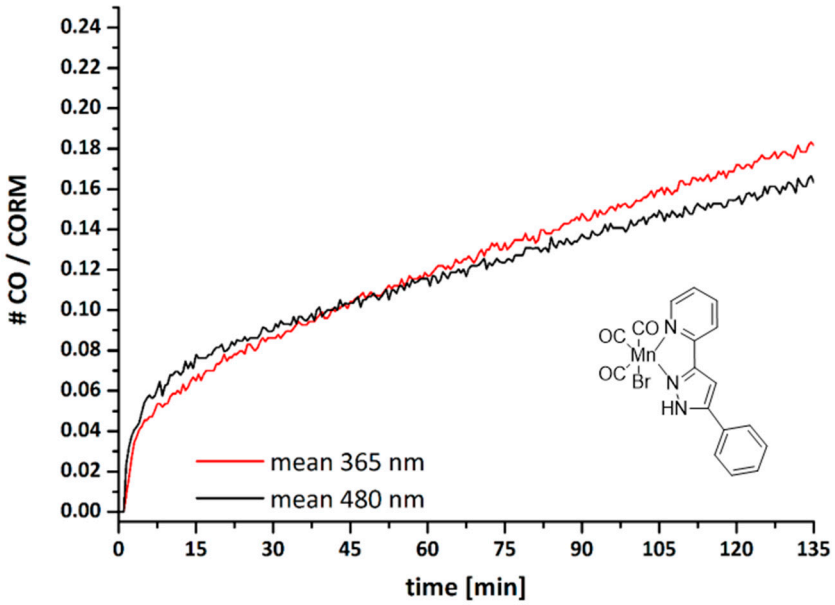

Figure 5. Carbon monoxide release kinetics upon illumination of crystalline $[(OC)_3Mn(Br)(2\text{-}PyPz^{Ph})]$ (**2a**) at 365 nm (**red**) and at 480 nm (**black**).

*2.4. Electrochemical Studies of $[(OC)_3Mn(Br)(2\text{-}PyPz^{Fc})]$ (**2k**)*

Electrochemical data were obtained by cyclic voltammetry using a conventional single-compartment three-electrode cell arrangement in combination with a potentiostat "AUTOLAB, eco chemie". As electrodes, the following were used: auxiliary electrode (0.196 cm^2 Pt disk electrode), working electrode (glassy carbon), and Ag/AgCl reference electrode (Ag/AgCl (LiCl sat.)). The Ag/AgCl electrode comprised a AgCl coated Ag wire in the same electrolyte solution, separated from the solution by a frit, and was prevent leakage of Ag^+ ions into the solution. The measurements were carried out in anhydrous and nitrogen purged acetonitrile with 0.1 M terabutylammonium tetrafluoroborate (recrystallized twofold) as supporting electrolyte and analyt concentration of 3×10^{-4} mol/L. All potentials are referenced by the ferrocenium/ferrocene couple ($E(Fc/Fc^+)$ = 0.48 V). All experiments were performed at room temperature.

The cyclic voltammogram of **1k** (Figure 6, top) shows a half-wave potential of $E_{1/2}(Fc/Fc^+)$ 0.08 V versus Fc/Fc^+, whereas a slight shift is observed in the carbonylmanganese(I) complex **2k** with $E_{1/2}(Fc/Fc^+)$ 0.11 V versus Fc/Fc^+. Furthermore, the voltammogram of **2k** exhibits two irreversible, consecutive anodic waves at $E_p{}^a$ 0.63 and 0.78 V versus Fc/Fc^+. These irreversible oxidation processes result from the oxidation of manganese(I) to manganese(II) and of bromide to bromine, respectively. This observation agrees well with the electrochemical characterization of the ferrocenyl-free photoCORM-EDE1, $[(OC)_3Mn(\mu\text{-}SCH_2CH_2NH_3)_3Mn(CO)_3]Br_2$; however, due to the dinuclear nature of the latter compound, two consecutive Mn^+/Mn^{2+} potentials have been found.

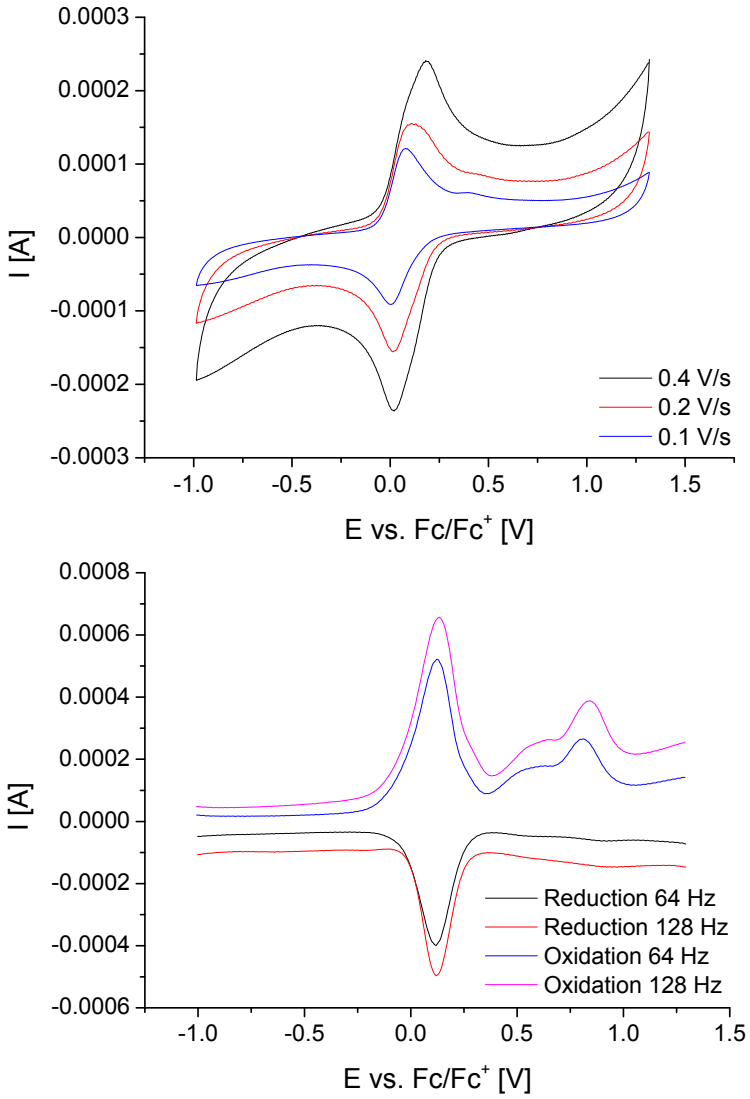

Figure 6. Cyclovoltammogram of **1k** (top) and square-wave voltammogram of **2k** (bottom) in acetonitrile/$TBABF_4$.

3. Discussion

The pyridylpyrazoyles with substituents in 5-position bind as a bidentate ligand to the 14-electron $(OC)_3MnBr$ units. Regardless of this substitution the $^{13}C\{^1H\}$ NMR shifts of the carbonyl ligands vary in a very narrow range. Furthermore, the IR stretching frequencies of the carbonyl groups are very similar. This finding offers the possibility to vary the periphery of the manganese(I) complex to tune properties with negligible influence on the central $(OC)_3MnBr$ moiety. Alkyl and aryl groups with different bulkiness are accepted as well as functionalized aryl groups.

Degradation of these manganese(I)-based photoCORMs leads to oxidation of the manganese center to di- or trivalent metal atoms. These oxidized manganese species are unable to bind carbon monoxide and hence, carbonyl-free and tetranuclear cage compounds are observed. This finding agrees well with the electrochemical studies at the ferrocenyl-substituted complex **2k**. The oxidation of the ferrocenyl substructure is reversible whereas the oxidation of the manganese(I) center is an irreversible process. Both redox steps occur independently of each other, verifying that the substituent in 5-position shows only negligible influence on the central manganese(I) carbonyl fragment.

4. Materials and Methods

4.1. General Remarks

All manipulations were carried out in an inert nitrogen atmosphere using standard Schlenk techniques. The solvents were dried according to standard procedures over KOH and subsequently distilled over sodium/benzophenone in a nitrogen atmosphere prior to use. Deuterated solvents were dried over sodium, degassed, and saturated with nitrogen. The yields given are not optimized. ^{1}H and ^{13}C{^{1}H} NMR spectra were recorded on Bruker AC 400 and AC 600 spectrometers (Bruker AXS GmbH, Karlsruhe, Germany). Chemical shifts are reported in parts per million relative to $SiMe_4$ as external standard. The residual signals of the deuterated solvents were used as internal standards for ^{1}H and ^{13}C{^{1}H} NMR experiments. Commercially available chemicals were purchased from Sigma-Aldrich (Sigma-Aldrich Chemie GmbH, Munich, Germany) or Alfa Aesar (Thermo Fisher GmbH, Karlsruhe, Germany).

4.2. General Procedures

Only the general procedures are given, more detailed descriptions are presented in the Supporting Information.

Method A (**2a** to **2g**): The appropriate pyridylpyrazole **1** was suspended in methanol. In another flask, a stoichiometric or a slight excess of $Mn(CO)_5Br$ was dissolved in methanol and transferred at once to the suspension of **1**. Then the reaction mixture was refluxed for several hours whereby a solid precipitated. The reaction mixture was cooled to room temperature. The precipitate was collected, washed with a few mL of methanol and dried in vacuo. The yields varied between 60% and a nearly quantitative conversion.

Method B (**2h** to **2l**): The suspension of $Mn(CO)_5Br$ and the appropriate pyridylpyrazole **1** in diethyl ether was refluxed for several hours until gas evolution ceased. During this time, a solid precipitated. Then the reaction mixture was cooled to room temperature. The precipitate was collected, washed with a few mL of cold diethyl ether and dried in vacuo.

4.3. X-Ray Structure Determinations

The intensity data for the compounds were collected on a Nonius KappaCCD diffractometer using graphite-monochromated Mo-Kα radiation. Data were corrected for Lorentz and polarization effects; absorption was taken into account on a semi-empirical basis using multiple-scans [37–39]. The structures were solved by Direct Methods (SHELXS [40]) and refined by full-matrix least squares techniques against F_o^2 (SHELXL-97 [40]). The hydrogen atoms were included at calculated positions with fixed thermal parameters for **1e**, **2b** (with exception of the amine hydrogen atom bonded to N3), for the disordered thiophene carbon atom C10 and the methyl groups of the methanol molecules of **2j**, **3a** and **3b** (with exception of the OH-groups of the methanol molecules). All other hydrogen atoms were located by difference Fourier synthesis and refined isotropically. All non-hydrogen atoms were refined anisotropically [40]. The crystal of **2g** contained large voids, filled with disordered solvent molecules. The size of the voids were 81 Å^3/unit cell. Their contribution to the structure factors was secured by back-Fourier transformation using the SQUEEZE routine of the program PLATON [41] resulting in 17 electrons/unit cell. Crystallographic data as well as structure solution and refinement details are summarized in Table S1. XP [42] and POV-Ray [43] were used for representations of molecular structures.

5. Conclusions

In this research project, we demonstrated that pyridylpyrazoles with a substituent in 5-position represent valuable photoCORMs. The influence of the 5-substitution on the 14-electron $(OC)_3MnBr$ fragment is negligible allowing to modify this group according to future requirements

(such as e.g., tracing of these photoCORMs via vibrational or fluorescence spectroscopy as well as tuning of the solubility in physiological solutions).

Supplementary Materials: The following are available online at www.mdpi.com/2304-6740/5/1/8/s1, Figures S1–S3 and S5–S12: molecule representations, Figures S4 and S15: UV-Vis spectra, Figures S13 and S14: cyclovoltammetric measurements; Table S1: Crystal data and refinement details of the X-ray structure determinations; preparative details, yields and spectroscopic data. Crystallographic data (excluding structure factors) has been deposited with the Cambridge Crystallographic Data Centre as supplementary publication CCDC-1520243 for **1e**, CCDC-1520244 for **1f**, CCDC-1520245 for **2a**, CCDC-1520246 for **2b**, CCDC-1520247 for **2e**, CCDC-1520248 for **2f**, CCDC-1520249 for **2g**, CCDC-1520250 for **2h**, CCDC-1520251 for **2i**, CCDC-1520252 for **2j**, CCDC-1520253 for **2k**, CCDC-1520254 for **3a**, and CCDC-1520255 for **3b**. Copies of the data can be obtained free of charge on application to CCDC, 12 Union Road, Cambridge CB2 1EZ, UK (E-mail: deposit@ccdc.cam.ac.uk).

Acknowledgments: This research project was funded by the German Research Foundation (DFG, Bonn, Germany) in the frame of the Collaborative Researcher Group FOR 1738. In addition, we thank the Fonds der Chemischen Industrie im Verband der Chemischen Industrie (FCI/VCI, Frankfurt/Main, Germany, fund no. 510259). We acknowledge the valuable support by Christoph Müller and Tina Schlotthauer.

Author Contributions: Ralf Mede, Steve Gläser, Benedikt Suchland, and Miles Mandel conceived and performed the experiments; Björn Schowtka developed a high-yield synthesis for 5-substituted pyridylpyrazoles **1**; Helmar Görls performed the X-ray crystal structures at single crystals and interpreted the data sets; Ralf Mede and Steve Gläser analyzed the spectroscopic data and studied the CO release; Sven Krieck performed all electrochemical studies; design of the experiments, supervision was performed by Alexander Schiller and Matthias Westerhausen; Ralf Mede and Matthias Westerhausen organized the manuscript.

Conflicts of Interest: The authors declare no conflict of interest.

References

1. Ji, X.; Damera, K.; Zheng, Y.; Yu, B.; Otterbein, L.E.; Wang, B. Toward Carbon Monoxide-Based Therapeutics: Critical Drug Delivery and Development Issues. *J. Pharmaceut. Sci.* **2016**, *105*, 406–416. [CrossRef] [PubMed]
2. Marhenke, J.; Trevino, K.; Works, C. The Chemistry, Biology and Design of Photochemical CO Releasing Molecules and the Efforts to detect CO for Biological Applications. *Coord. Chem. Rev.* **2016**, *306*, 533–543. [CrossRef]
3. Inaba, H.; Fujita, K.; Ueno, T. Design of Biomaterials for Intracellular Delivery of Carbon Monoxide. *Biomater. Sci.* **2015**, *3*, 1423–1438. [CrossRef] [PubMed]
4. Schatzschneider, U. Novel Lead Structures and Activation Mechanisms for CO-Releasing Molecules (CORMs). *Br. J. Pharmacol.* **2015**, *172*, 1638–1650. [CrossRef] [PubMed]
5. Chakraborty, I.; Carrington, S.J.; Mascharak, P.K. Design Strategies to Improve the Sensitivity of Photoactive Metal Carbonyl Complexes (photoCORMs) to Visible Light and Their Potential as CO-Donors to Biological Targets. *Acc. Chem. Res.* **2014**, *47*, 2603–2611. [CrossRef] [PubMed]
6. Heinemann, S.H.; Hoshi, T.; Westerhausen, M.; Schiller, A. Carbon Monoxide—Physiology, Detection and Controlled Release. *Chem. Commun.* **2014**, *50*, 3644–3660. [CrossRef] [PubMed]
7. García-Gallego, S.; Bernardes, G.J.L. Carbon-Monoxide-Releasing Molecules for the Delivery of Therapeutic CO in Vivo. *Angew. Chem. Int. Ed.* **2014**, *53*, 9712–9721. [CrossRef] [PubMed]
8. Gonzales, M.A.; Mascharak, P.K. Photoactive Metal Carbonyl Complexes as Potential Agents for Targeted CO Delivery. *J. Inorg. Biochem.* **2014**, *133*, 127–135. [CrossRef] [PubMed]
9. Foresti, R.; Motterlini, R. CO-Releasing Molecules: Avoiding Toxicity and Exploiting the Beneficial Effects of CO for the Treatment of Cardiovascular Disorders. *Future Med. Chem.* **2013**, *5*, 367–369. [CrossRef] [PubMed]
10. Zobi, F. CO and CO-releasing Molecules in Medicinal Chemistry. *Future Med. Chem.* **2013**, *5*, 175–188. [CrossRef] [PubMed]
11. Romão, C.C.; Blättler, W.A.; Seixas, J.D.; Bernardes, G.J.L. Developing Drug Molecules for Therapy with Carbon Monoxide. *Chem. Soc. Rev.* **2012**, *41*, 3571–3583. [CrossRef] [PubMed]
12. Mann, B.E. CO-releasing Molecules: A Personal View. *Organometallics* **2012**, *31*, 5728–5735. [CrossRef]
13. Rimmer, R.D.; Pierri, A.E.; Ford, P.C. Photochemically Activated Carbon Monoxide Release for Biological Targets. Toward Developing Air-Stable photoCORMs Labilized by Visible Light. *Coord. Chem. Rev.* **2012**, *256*, 1509–1519. [CrossRef]

14. Schatzschneider, U. PhotoCORMs: Light-Triggered Release of Carbon Monoxide from the Coordination Sphere of Transition Metal Complexes for Biological Applications. *Inorg. Chim. Acta* **2011**, *374*, 19–23. [CrossRef]
15. Schatzschneider, U. Photoactivated Biological Activity of Transition-Metal Complexes. *Eur. J. Inorg. Chem.* **2010**, 1451–1467. [CrossRef]
16. Motterlini, R.; Otterbein, L.E. The Therapeutic Potential of Carbon Monoxide. *Nat. Rev.* **2010**, *9*, 728–743. [CrossRef] [PubMed]
17. Mann, B.E. Carbon Monoxide: An Essential Signalling Molecule. *Top. Organomet. Chem.* **2010**, *32*, 247–285.
18. Barry, N.P.E.; Sadler, P.J. Exploration of the Medical Periodic Table: Towards New Targets. *Chem. Commun.* **2013**, *49*, 5106–5131. [CrossRef] [PubMed]
19. Kaim, W.; Schwerderski, B. *Bioinorganic Chemistry: Inorganic Elements in the Chemistry of Life: An Introduction and Guide*; Wiley: Chichester, UK, 1994.
20. Frausto da Silva, J.J.R.; Williams, R.J.P. *The Biological Chemistry of the Elements: The Inorganic Chemistry of Life*, 2nd ed.; Oxford University Press: Oxford, UK, 2001.
21. Maret, W. *Metallomics: A Primer of Integrated Biometal Sciences*; Imperial College Press: London, UK, 2016.
22. Costa, L.G.; Aschner, M. (Eds.) *Manganese in Health and Disease*; The Royal Society of Chemistry: Cambridge, UK, 2015.
23. Mede, R.; Lorett-Velásquez, V.P.; Klein, M.; Görls, H.; Schmitt, M.; Gessner, G.; Heinemann, S.H.; Popp, J.; Westerhausen, M. Carbon Monoxide Release Properties and Molecular Structures of Thiophenolatomanganese(I) Carbonyl Complexes of the Type $[(OC)_4Mn(\mu\text{-S-aryl})]_2$. *Dalton Trans.* **2015**, *44*, 3020–3033. [CrossRef] [PubMed]
24. Kautz, A.C.; Kunz, P.C.; Janiak, C. CO-Releasing Molecule (CORM) Conjugate Systems. *Dalton Trans.* **2016**, *45*, 18045–18063. [CrossRef] [PubMed]
25. Nguyen, D.; Boyer, C. Macromolecular and Inorganic Nanomaterials Scaffolds for Carbon Monoxide Delivery: Recent Developments and Future Trends. *ACS Biomater. Sci. Eng.* **2015**, *1*, 895–913. [CrossRef]
26. Gläser, S.; Mede, R.; Görls, H.; Seupel, S.; Bohlender, C.; Wyrwa, R.; Schirmer, S.; Dochow, S.; Reddy, G.U.; Popp, J.; et al. Remote-Controlled Delivery of CO via Photoactive CO-Releasing Materials on a Fiber Optical Device. *Dalton Trans.* **2016**, *45*, 13222–13233. [CrossRef] [PubMed]
27. Bohlender, C.; Gläser, S.; Klein, M.; Weisser, J.; Thein, S.; Neugebauer, U.; Popp, J.; Wyrwa, R.; Schiller, A. Light-Triggered CO Release from Nanoporous Non-Wovens. *J. Mater. Chem. B* **2014**, *2*, 1454–1463. [CrossRef]
28. Mede, R.; Klein, M.; Claus, R.A.; Krieck, S.; Quickert, S.; Görls, H.; Neugebauer, U.; Schmitt, M.; Gessner, G.; Heinemann, S.H.; et al. CORM-EDE1: A Highly Water-Soluble and Nontoxic Manganese-Based photoCORM with a Biogenic Ligand Sphere. *Inorg. Chem.* **2016**, *55*, 104–113. [CrossRef] [PubMed]
29. Dördelmann, G.; Pfeiffer, H.; Birkner, A.; Schatzschneider, U. Silicium Dioxide Nanoparticles as Carriers for Photoactivatable CO-Releasing Molecules (PhotoCORMs). *Inorg. Chem.* **2011**, *50*, 4362–4367. [CrossRef] [PubMed]
30. Dördelmann, G.; Meinhardt, T.; Sowik, T.; Krueger, A.; Schatzschneider, U. CuAAC Click Functionalization of Azide-Modified Nanodiamond with a Photoactivatable CO-Releasing Molecule (PhotoCORM) Based on $[Mn(CO)_3(tpm)]^+$. *Chem. Commun.* **2012**, *48*, 11528–11530. [CrossRef] [PubMed]
31. Mukherjee, R. Coordination Chemistry with Pyrazole-Based Chelating Ligands: Molecular Structural Aspects. *Coord. Chem. Rev.* **2000**, *203*, 151–218. [CrossRef]
32. Schowtka, B.; Görls, H.; Westerhausen, M. 3-(1-Adamantyl)-, 3-Ferrocenyl- and 3-(2-Furanyl)-Substituted 5-(2-Pyridyl)pyrazole as Well as Lithium and Zinc Complexes. *Z. Anorg. Allg. Chem.* **2014**, *640*, 907–915. [CrossRef]
33. Schowtka, B.; Müller, C.; Görls, H.; Westerhausen, M. Synthesis, Structures and Spectroscopic Properties of 3-Aryl-5-(2-pyridyl)pyrazoles and Related Pyrazoles. *Z. Anorg. Allg. Chem.* **2014**, *640*, 916–925. [CrossRef]
34. Reyes-Lezama, M.; Höpfl, H.; Zúñiga-Villarreal, N. Tricarbonyl[(1–5-η)-pentadienyl]manganese: A Source of Benzeneselenatomanganese Derivatives of Diverse Nuclearity. *Organometallics* **2010**, *29*, 1537–1540. [CrossRef]
35. Germán-Acacio, J.M.; Reyes-Lezama, M.; Zúñiga-Villarreal, N. Synthesis and Structural Studies of Phosphorus Carbonyl Manganacycles Containing the Tetraphenyldiselenoimidodiphosphinato Ligand. *J. Organomet. Chem.* **2006**, *691*, 3223–3231. [CrossRef]

36. Herrmann, W.A.; Serrano, R.; Weichmann, J. Metallcarbonyl Synthesen XIII. Eine Mangan–Mangan-Dreifachbindung. *J. Organomet. Chem.* **1983**, *246*, C57–C60. [CrossRef]
37. Hooft, R. *COLLECT, Data Collection Software*; Nonius B.V.: Rotterdam, The Netherlands, 1998.
38. Otwinowski, Z.; Minor, W. Processing of X-Ray Diffraction Data Collected in Oscillation Mode. In *Methods in Enzymology, Macromolecular Crystallography*; Carter, C.W., Sweet, R.M., Eds.; Academic Press: New York, NY, USA, 1997; Part A; Volume 276, pp. 307–326.
39. *SADABS 2.10*; Bruker-AXS Inc.: Madison, WI, USA, 2002.
40. Sheldrick, G.M. A Short History of SHELX. *Acta Cryst.* **2008**, *A64*, 112–122. [CrossRef] [PubMed]
41. Spek, A.L. Structure Validation in Chemical Crystallography. *Acta Cryst.* **2009**, *D65*, 148–155. [CrossRef] [PubMed]
42. *XP*; Siemens Analytical X-ray Instruments Inc.: Karlsruhe, Germany, 1990; Madison, WI, USA, 1994.
43. *POV-Ray*; Persistence of Vision Raytracer: Victoria, Australia, 2007.